Mechanisms for spin supersolidity in $S=\frac{1}{2}$ spin-dimer antiferromagnets

J.-D. Picon,[1,2] A. F. Albuquerque,[1,3] K. P. Schmidt,[4] N. Laflorencie,[5] M. Troyer,[1] and F. Mila[2]
[1]*Theoretische Physik, ETH Zürich, 8093 Zürich, Switzerland*
[2]*Institute of Theoretical Physics, EPF Lausanne, 1015 Lausanne, Switzerland*
[3]*School of Physics, The University of New South Wales, Sydney, New South Wales 2052, Australia*
[4]*Lehrstuhl für Theoretische Physik I, TU Dortmund, Otto-Hahn-Straße 4, D-44221 Dortmund, Germany*
[5]*Laboratoire de Physique des Solides, Université Paris-Sud, UMR-8502 CNRS, 91405 Orsay, France*
(Received 31 July 2008; revised manuscript received 15 October 2008; published 17 November 2008)

Using perturbative expansions and the contractor renormalization (CORE) algorithm, we obtain effective hard-core bosonic Hamiltonians describing the low-energy physics of $S=1/2$ spin-dimer antiferromagnets known to display supersolid phases under an applied magnetic field. The resulting effective models are investigated by means of mean-field analysis and quantum Monte Carlo simulations. A "leapfrog mechanism," through means of which extra singlets delocalize in a checkerboard-solid environment via correlated hoppings, is unveiled that accounts for the supersolid behavior.

DOI: 10.1103/PhysRevB.78.184418 PACS number(s): 03.75.Nt, 05.30.Jp, 75.10.Jm, 75.40.Mg

I. INTRODUCTION

Concepts and techniques developed within a well established research field are often employed in exploring physics displayed by apparently unrelated systems. Following this trend, there has been an increased interest in field-induced Bose-Einstein condensation of magnons in quantum magnets (for a recent review, see Ref. 1). Although the analogy is never complete, this line of research undoubtedly has led to considerable success in unveiling phenomena in a growing number of magnetic insulators under applied magnetic field. The success of this approach suggests that one might be able to experimentally observe more elusive bosonic behavior in quantum magnets, such as the phase simultaneously displaying diagonal and off-diagonal order known as *supersolid*.

Supersolidity has attracted enormous interest since the detection of nonclassical rotational inertia in solid helium by Kim and Chan.[2,3] Although the correct interpretation of these measurements is still hotly debated and there seems to be no consensus on the possibility of supersolidity in translationally invariant systems,[4–7] the occurrence of supersolid phases for bosonic models on a lattice is a well established fact. While the simplest model of interacting hard-core bosons on a square lattice is unstable against phase separation, which prevents supersolid behavior,[8–10] it has been shown that frustration,[11–14] removal of the hard-core constraint,[10,15] or inclusion of generalized couplings in the Hamiltonian[16,17] can stabilize supersolidity. Although a more direct implementation of these models remains elusive, due to the short-ranged nature of interactions between atoms in optical lattices, one might expect that they are relevant in the context of quantum magnets under an applied magnetic field.

Indeed, as it was first shown by Ng and Lee[18] and further verified by some of us,[19] an $S=1/2$ spin-dimer model on the square lattice with intraplane coupling Ising-type anisotropy [see Eq. (1) below] has a phase simultaneously displaying diagonal and off-diagonal order, the equivalent of a supersolid for spin systems (henceforth dubbed *spin supersolid*). Later spin supersolidity was also shown to occur for $S=1$ systems on a bilayer[20] and on a chain.[21] However, the exact relationship between these spin models and the aforementioned bosonic lattice models is not well understood. For instance, one might naively expect that the $S=1/2$ spin-dimer model investigated in Refs. 18 and 19 will map onto a t-V model for hard-core bosons on a square lattice, which is known not to display a supersolid phase.[9,10] Therefore, in order to understand the mechanism behind supersolidity in this model one should analyze the presence of extra terms in the effective model.

Using a perturbative analysis and the contractor renormalization (CORE) method, we derive effective Hamiltonians for the $S=1/2$ spin-dimer model studied in Refs. 18 and 19. A mean-field (MF) analysis of the resulting generalized hard-core bosonic Hamiltonian leads to a minimal model capable of accounting for supersolid behavior, which is then studied by means of quantum Monte Carlo (QMC).

II. MODEL

We analyze the $S=1/2$ spin-dimer Hamiltonian analyzed by Ng and Lee[18] and some of us,[19] which reads

$$\mathcal{H} = J_\perp \sum_i \vec{S}_{i,1} \cdot \vec{S}_{i,2} - h \sum_{i,\alpha=1,2} S^z_{i,\alpha} + J \sum_{\langle i,j\rangle,\alpha=1,2} (S^x_{i,\alpha} S^x_{j,\alpha} + S^y_{i,\alpha} S^y_{j,\alpha} + \Delta S^z_{i,\alpha} S^z_{j,\alpha}). \quad (1)$$

$\vec{S}_{i,\alpha}$ is an $S=1/2$ operator attached to the site i of the layer α (see Fig. 1). $J_\perp$ couples spins in different layers and is considered to be the essential coupling, being responsible for the system's strong dimerized character (we set $J_\perp=1$ throughout the rest of the paper). Spins in the same layer interact via the coupling J and Δ is an Ising-type anisotropy; finally, the magnetic field h is applied along the easy axis. We will mainly focus on the set of parameters considered in Refs. 18 and 19, $J/J_\perp=0.29$ and $\Delta=3.3$, leading to an extended supersolid phase as evident from the QMC results for the spin stiffness ρ_s and static structure factor $S(\pi,\pi)$ obtained by Laflorencie and Mila[19] and reproduced in Fig. 2.

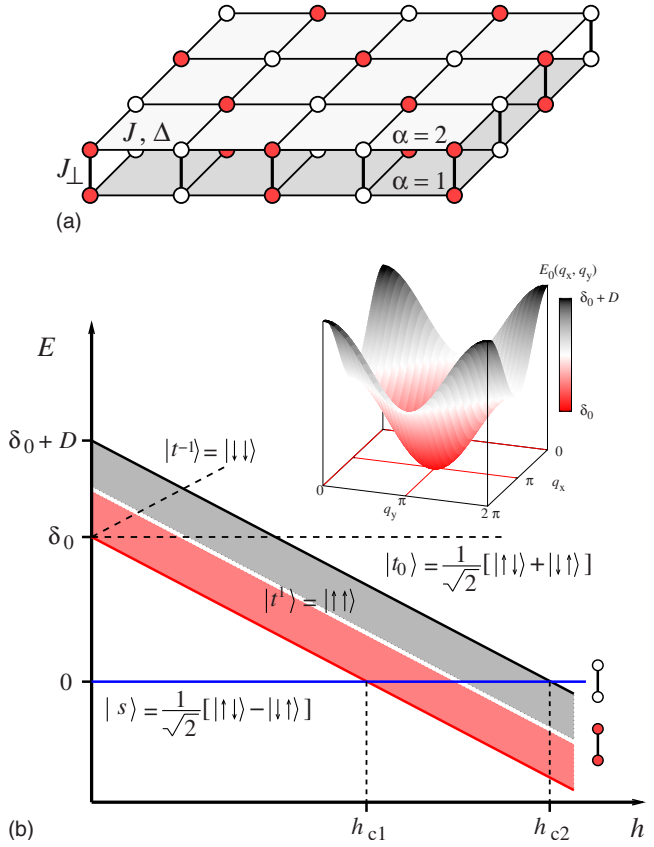

FIG. 1. (Color online) (a) The bilayer spin system investigated in this paper, described by the Hamiltonian of Eq. (1). The strong coupling $J_\perp$, represented by thick vertical lines, accounts for the system's strong dimer character. Application of a magnetic field along the z direction promotes dimers from a singlet ($|s\rangle$, vertical pairs of open circles) to a triplet ($|t^1\rangle$, pairs of filled circles) state and controls the density of emergent bosons as depicted in (b). Solid (and supersolid) phases might be stabilized for field values in the range between the lower-critical field h_{c1}, where the bottom of the triplet band (represented in the inset and separated from the singlet state by a zero-field gap δ_0 and with width D) and the singlet state become degenerate, and the upper-critical field h_{c2} where the system becomes fully polarized. In-plane coupling J leads to interactions and hopping amplitudes for emergent bosons, the anisotropy $\triangle$ being necessary to stabilize a checkerboard solid represented in the upper panel.

Our goal is to show that we can understand the emergence of SS for the spin model [Eq. (1)] in terms of simple microscopic mechanisms. In achieving this, we derive effective bosonic models for Eq. (1) by means of two different procedures: high-order perturbative series expansions and the contractor renormalization (CORE) algorithm. We are going to show that correlated hoppings for singlets (holes) with amplitudes $\tilde{s}_1$ [next-nearest-neighbor (NNN) hopping which occurs only if at least one of the other sites in the same plaquette is occupied] and $\tilde{s}_2$ (assisted next-nearest-neighbor hopping occurring only when the site in between is occupied), depicted in Figs. 3(a) and 3(b), respectively, are crucial in accounting for SS behavior for the model of Eq. (1). It is easy to see [Fig. 3(c)] that these processes prevent phase separation[10] in the hard-core bosonic model on the square

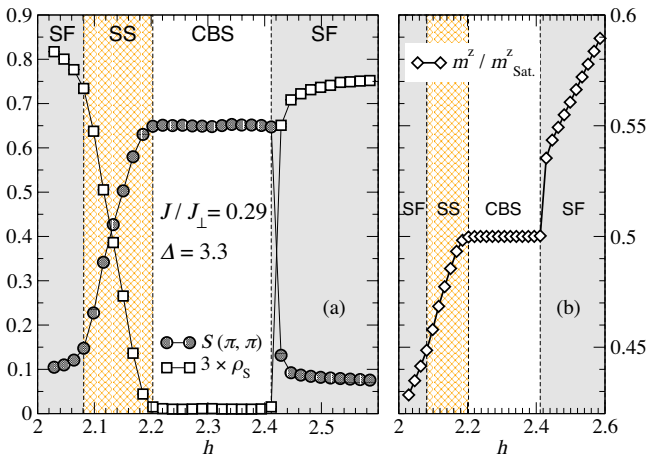

FIG. 2. (Color online) QMC results for the spin-dimer model [Eq. (1)]. Simulations were performed on a $16\times16\times2$ lattice with β=32, for $J/J_\perp$=0.29. (a) Spin stiffness ρ_s (open squares) and static structure factor $S(\pi,\pi)$ (filled circles) (Ref. 22). (b) Normalized magnetization per site $m^z/m^z_{\rm sat}$ (open diamonds), equivalent to particle density in the bosonic language. Different phases are stabilized as a function of the applied magnetic field, namely: a superfluid (SF) phase with finite ρ_s and vanishing structure factor, an extended supersolid (SS) in which both ρ_s and $S(\pi,\pi)$ are finite and a checkerboard solid (CBS). Error bars are much smaller than the depicted symbols (adapted from Ref. 19).

lattice (t-V model) by allowing extra singlets (holes) to delocalize in a checkerboard-solid (CBS) environment by "leapfrogging" on the other sublattice and forming a condensate. It is useful to define the quantity we call "leapfrog ratio,"

$$\Sigma = \frac{(2|\tilde{s}_1| + |\tilde{s}_2|)}{|\tilde{t}_1|}, \tag{2}$$

where $\tilde{t}_1$ is the nearest-neighbor (NN) hopping amplitude for holes. It was shown by Sengupta *et al.*[10] that the energetic gain in the domain wall formation behind phase separation in the t-V model is $c\tilde{t}_1$, where c lies in the interval [1, 2]. Therefore, for a system of hard-core bosons on the square lattice, the energetic gain associated to the correlated hoppings depicted in Fig. 3 must be larger than $c\tilde{t}_1$, implying that the

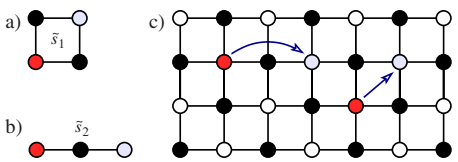

FIG. 3. (Color online) (a) NNN correlated hopping with amplitude $\tilde{s}_1$ and (b) third-neighbor correlated hopping with amplitude $\tilde{s}_2$: singlets (holes) hop in between red and light-blue sites *only* if the black-filled circles are occupied by holes [in (a), at least one of the sites must be occupied; if both are, the process occurs with amplitude $2\tilde{s}_1$]. This "leapfrog mechanism" allows for extra holes to delocalize in a checkerboard ordered environment, as illustrated in (c), and to condense, giving rise to supersolid behavior.

condition $\Sigma > c/4$ must be obeyed, for SS behavior to emerge.

III. PERTURBATIVE EXPANSIONS

Following the work of Totsuka[23] and Mila,[24] we restrict ourselves to the limit where $J_\perp$ is the main energy scale and the system consists of weakly coupled dimers. The application of a magnetic field lowers the energy of one of the triplet bands and at the critical field h_{c1} the singlet state $|s\rangle$ (holes) and the bottom of the triplet $|t^1\rangle$ (bosons) band become degenerate [see Fig. 1(b)]. By expanding the Hamiltonian Eq. (1) in terms of the small parameter $J/J_\perp$ we can thus obtain an effective hard-core bosonic model. Within first-order in $J/J_\perp$, the only effective couplings in the model obtained in this way are nearest-neighbor hopping amplitude t_1 and repulsion V_1 for the emergent bosons (triplets).[24] However, since this so-called t-V model [equivalent to Eq. (3) below if we set $s_{1,2}^{\mathrm{P2}}=0$] is known to display *no* SS phase,[8] higher-order effective couplings should be taken into account and we proceed to their derivation.

A. Second-order expansion

We extend the perturbative analysis of Mila[24] to second order in $J/J_\perp$, obtaining the following effective Hamiltonian:

$$\mathcal{H}_{\mathrm{eff}}^{\mathrm{P2}} = -\mu^{\mathrm{P2}} \sum_i n_i + \sum_{\langle i,j\rangle} [t_1^{\mathrm{P2}}(b_i^\dagger b_j + \mathrm{H.c.}) + V_1^{\mathrm{P2}} n_i n_j] + s_{1,2}^{\mathrm{P2}} \sum_{\langle i,j,k\rangle} [b_i^\dagger (1-n_j) b_k + \mathrm{H.c.}], \tag{3}$$

with effective couplings (we set $J_\perp = 1$)

$$\mu^{\mathrm{P2}} = 1 + \frac{J^2(2+\Delta^2)}{4} + h,$$

$$t_1^{\mathrm{P2}} = J/2, \quad s_{1,2}^{\mathrm{P2}} = -J^2/16,$$

$$V_1^{\mathrm{P2}} = \frac{J\Delta}{2} - \frac{J^2(2+\Delta^2)}{8}. \tag{4}$$

In Eq. (3), $n_i = b_i^\dagger b_i = \{0,1\}$ is the occupation number for hard-core bosons ($|t^1\rangle$ triplets) at the site i on the square lattice formed by the spin-dimers. $\langle i,j\rangle$ denotes NN sites on this lattice and $\langle i,j,k\rangle$ is such that j is a common nearest neighbor for the second- or third-neighbor sites i and k.[25] The physical processes at play become more evident after applying a particle-hole transformation, $(1-n_i) \to \tilde{n}_i$ and $b^\dagger \to \tilde{b}$, to Eq. (3):

$$\tilde{\mathcal{H}}_{\mathrm{eff}}^{\mathrm{P2}} = \tilde{\mu}^{\mathrm{P2}} \sum_i \tilde{n}_i + \sum_{\langle i,j\rangle} [t_1^{\mathrm{P2}}(\tilde{b}_i^\dagger \tilde{b}_j + \mathrm{H.c.}) + V_1^{\mathrm{P2}} \tilde{n}_i \tilde{n}_j] + s_{1,2}^{\mathrm{P2}} \sum_{\langle i,j,k\rangle} (\tilde{b}_i^\dagger \tilde{n}_j \tilde{b}_k + \mathrm{H.c.}). \tag{5}$$

We have ignored constant terms and $\tilde{\mu}^{\mathrm{P2}} = \mu^{\mathrm{P2}} + 2V_1^{\mathrm{P2}}$; $\tilde{n}_i = \tilde{b}_i^\dagger \tilde{b}_i$ is now the *singlet* (holes) occupation number. In addition to the first-order couplings t_1^{P2} (NN hopping amplitude) and V_1^{P2} (NN repulsion) the second-order effective Hamiltonian also contains a correlated hopping term with amplitude $s_{1,2}^{\mathrm{P2}}$ [see Figs. 3(a) and 3(b)].[25] Correlated hoppings have been shown to stabilize supersolidity[17] by allowing particles to delocalize in a CBS ordered background. However, the second-order amplitude for correlated hoppings is too small[10,17] to prevent phase separation: the "leapfrog ratio" of Eq. (2), $\Sigma^{\mathrm{P2}} = 3J/8 \approx 0.12$ for $J/J_\perp = 0.29$ is too small and cannot account for supersolidity. Therefore we extend our analysis and include higher-order corrections to the parameters t_1^{P2}, V_1^{P2}, and $s_{1,2}^{\mathrm{P2}}$ in Eq. (5) with the help of perturbative continuous unitary transformations (PCUTs).

B. PCUTs

The method of continuous unitary transformations (CUTs) (Refs. 26–29) in its perturbative variant[30–33] and quasiparticle conserving form is an efficient tool to derive effective low-energy models for coupled quantum dimer networks in a magnetic field up to high order in perturbation.[34,35] To this end, the original spin Hamiltonian Eq. (1) is rewritten in terms of rung triplet operators $t_\alpha^{(\dagger)}$ with $\alpha = \{\pm 1, 0\}$. This Hamiltonian does not conserve the number of triplets $Q = \sum_{i,\alpha=\pm1,0} t_\alpha^\dagger t_\alpha$ in the system. The basic idea of quasiparticle conserving CUTs is to transform $\mathcal{H}$ into $\mathcal{H}_{\mathrm{eff}}$ such that $[\mathcal{H}_{\mathrm{eff}}, Q] = 0$; i.e., the number of quasiparticles (triplons, in the present case) is a conserved quantity. Since the total S_{tot}^z is also a conserved quantity, the magnetic field term does *not* change under the unitary transformation. For the case of coupled dimers in a magnetic field, one can therefore restrict to terms in $\mathcal{H}_{\mathrm{eff}}$ consisting solely of triplet operators $t_1^{(\dagger)}$ in order to describe the low-energy physics.

In general, a continuous parameter l is introduced such that $l=0$ refers to the initially given system $\mathcal{H}$ and $l=\infty$ corresponds to the final effective system $\mathcal{H}_{\mathrm{eff}}$. Let U be the unitary transformation which diagonalizes the Hamiltonian $\mathcal{H}$ and $\mathcal{H}(l) = U^\dagger(l)\mathcal{H}U(l)$. Then this unitary transformation is equivalent to performing an infinite sequence of unitary transforms $e^{-\eta(l)dl}$ with the anti-Hermitian generator

$$\eta(l) = -U^\dagger(l)\partial_l U(l). \tag{6}$$

The derivation with respect to l results in the so-called flow equation

$$\partial_l \mathcal{H}(l) = [\eta(l), \mathcal{H}(l)], \tag{7}$$

which defines the change of the Hamiltonian during the flow. The properties of the effective Hamiltonian depend strongly on the choice of the generator η. Quasiparticle-conserving CUTs chooses η such that the Hamiltonian $\mathcal{H}_0$ maps onto an effective Hamiltonian which *conserves* the number of quasiparticles.[30–33]

In the following we consider the limit of weakly coupled rung dimers; i.e., we set $J_\perp = 1$ and treat J and Δ as small expansion parameters. Using a series expansion ansatz for η and $\mathcal{H}$ in Eq. (7), one can derive the effective quasiparticle conserving Hamiltonian up to high order in perturbation.[30,33,36] The results are obtained in the thermodynamic limit and in second quantization.

We stress again that the total S_{tot}^z is a conserved quantity.

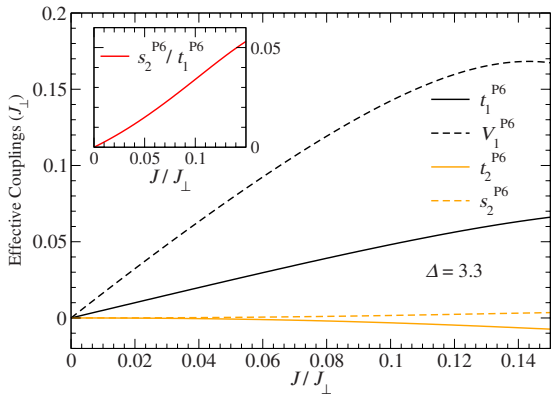

FIG. 4. (Color online) $\Delta=3.3$. Effective couplings obtained from the PCUTs procedure described in the main text: nearest-neighbor hopping amplitude t_1^{P6} (solid dark line) and interaction V_1^{P6} (dashed dark line) and amplitudes for next-nearest-neighbor uncorrelated (t_2^{P6}, solid light line) and correlated (s_2^{P6}, dashed light line) hoppings, as a function of $J/J_\perp$. The inset shows the dependence of the ratio s_2^{P6}/t_1^{P6} on $J/J_\perp$.

The magnetic field term has *not* changed under the unitary transformation and the low-energy physics is solely influenced by the local singlet $|s\rangle$ and the triplet $|t^1\rangle$ polarized parallel to the magnetic field (as discussed before). Identifying $|s\rangle$ with an empty site and $|t^1\rangle$ with the presence of a hard-core boson (as before), we can deduce the effective Hamiltonian in this language by calculating matrix elements on finite clusters.[36]

We have extended the derivation of the effective parameters appearing in Eq. (5), now relabeled as t_1^{P6}, V_1^{P6}, and s_2^{P6}, to sixth order in $J/J_\perp$ and have additionally calculated the amplitude t_2^{P6} for uncorrelated next-nearest-neighbor hopping. Explicit formulas are given in Appendix A and dependences on $J/J_\perp$ are shown in Fig. 4 for $\Delta=3.3$. Comparison between t_1^{P6} and results obtained from CORE (see Fig. 6 and discussion below) suggests that our perturbative analysis remains valid up to $J/J_\perp \lesssim 0.15$.

By applying a particle-hole transformation it is possible to show that the condition $t_2^{P6}=-2s_2^{P6}$, approximately fulfilled by our results (Fig. 4), implies a vanishing amplitude for *uncorrelated* next-nearest-neighbor hopping for *holes* (singlets) and therefore the magnitude of s_2^{P6} is the relevant kinetic scale for supersolidity (a similar situation happens for the effective Hamiltonian derived from CORE; see Sec. V A). As we mentioned before, supersolid behavior is expected to occur for large enough values of s_2^{P6}/t_1^{P6}.[10,17] However, our results for this ratio, shown in the inset of Fig. 4, are clearly too small for preventing domain-wall formation,[10,17] and therefore one does not expect to reproduce the extended SS phase observed for the original spin model, Eq. (1). Consequently, either our idea that the model can be described by only taking into account $|s\rangle$ and $|t^1\rangle$ is wrong, or we must go beyond a perturbative analysis. Since according to Ng and Lee[18] contributions from the other two triplets states $|t^0\rangle$ and $|t^{-1}\rangle$, if nonzero, are negligible close to half-filling, we therefore resort to a nonperturbative approach to our problem, namely the CORE algorithm.

IV. CONTRACTOR RENORMALIZATION

The CORE method was introduced by Morningstar and Weinstein[37,38] and has been recently[39] applied to the study of the spin-dimer Hamiltonian described by Eq. (1). We extend these results by considering the next range in the effective couplings and analyzing in more detail the resulting effective bosonic model.

A. Procedure

The basic idea behind CORE (for comprehensive accounts the reader is referred to Refs. 40 and 41) is to *project out* high energy degrees of freedom and to derive an effective Hamiltonian describing the low-energy physics of the original model. Usually this is done by first decomposing the lattice on which the original model is defined into elementary blocks and diagonalizing the Hamiltonian on a single block. After choosing a suitable number of low-energy block states, the model is subsequently diagonalized on a cluster consisting of a few elementary blocks and the lowest energy cluster states are projected onto the restricted basis formed by the tensor products of the retained block states. An effective Hamiltonian is then obtained by imposing the constraint that the low-energy spectrum of the full problem is exactly reproduced and by subtracting shorter-range contributions obtained from previous steps involving lesser blocks. The validity of the procedure can be checked by either analyzing the magnitude of long-range effective couplings (large values associated to these signal the inadequacy of the chosen restricted set of degrees of freedom in accounting for the system's low-energy behavior) or, perhaps more accurately, by keeping track of the weight of the reduced density matrix associated to a single block.[39,42]

For the spin-dimer model considered here, Eq. (1), large values for the interplane coupling $J_\perp$ imply that the natural choice when applying CORE is to consider the dimers as the elementary blocks: dimer singlet states, $|s\rangle$, corresponding to an unoccupied site in the effective model living on the square lattice, and an emergent boson created by promoting one singlet to an $S^z=1$ triplet state, $|t^1\rangle$, are the retained block states. The adequacy of this reduced set of degrees of freedom in describing the Hamiltonian of Eq. (1) in the regime known[18,19] to display supersolid behavior was verified by Abendschein and Capponi[39] and is confirmed in the present work.

Our results are obtained from the analysis of the clusters depicted in Fig. 5. They are labeled according to the maximum range for the effective couplings: *range*-1 are the results obtained from the analysis of the cluster containing two dimers shown in Fig. 5(a), *range*-$2^{1/2}$ denote the ones from the cluster with four dimers arranged as a plaquette [Fig. 5(b)] and *range*-2 results from the three-dimer cluster shown in Fig. 5(c). We gauge the validity of the mapping onto a system of hard-core bosons by analyzing corrections to the NN hopping amplitude t_1 (for *particles*) obtained from range-$2^{1/2}$ and range-2 CORE calculations: whenever the sum of these contributions exceeds the value obtained from range-1 CORE we *assume* that a valid mapping is not obtained. While the criteria used by Abendschein and

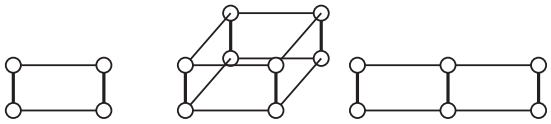

FIG. 5. Clusters used in the CORE derivation of the effective model, labeled according to the longest range effective couplings on the square lattice. In this convention, range-1 interactions are obtained from the analysis of the cluster consisting of two dimers (a), range-$2^{1/2}$ from the cluster with four dimers forming a square plaquette (b) and range-2 by considering three dimers along a line (c).

Capponi[39] is probably more accurate, our results agree qualitatively with theirs and suffice for our analysis. More importantly, for the parameters ($\Delta=3.3$ and $J/J_\perp=0.29$, vertical dashed line in Fig. 6) leading to supersolidity previously considered in the literature[18,19] both criteria validate the mapping onto the effective bosonic model.

The effective hard-core bosonic Hamiltonian obtained from the CORE calculation is, after applying a particle-hole transformation $(1-n_i)\rightarrow\tilde{n}_i$ and $b^\dagger\rightarrow\tilde{b}$, given by

$$\tilde{\mathcal{H}}^{\mathrm{C}}_{\mathrm{eff}}=\sum_i\{-\tilde{\mu}^{\mathrm{C}}\tilde{n}_i+[\tilde{\mathcal{V}}_i+\tilde{\mathcal{W}}_i]+[\tilde{\mathcal{T}}_i+\tilde{\mathcal{S}}_i+\tilde{\mathcal{R}}_i]\},\qquad(8)$$

where $\tilde{\mu}^{\mathrm{C}}$ is the chemical potential for the *holes* (singlets). $\tilde{\mathcal{V}}$ comprises two-body interactions and $\tilde{\mathcal{W}}$ three- and four-body interactions; $\tilde{\mathcal{T}}$, $\tilde{\mathcal{S}}$, and $\tilde{\mathcal{R}}$ are the kinetic contributions: direct and correlated hopping terms. Full expressions for each of these terms are given in Appendix B.

B. Comparison with perturbative expansion

Figure 6 shows our results for the effective nearest-neighbor hopping amplitude t_1 (for *particles*) obtained from CORE (range-1, -$2^{1/2}$, and -2) and from PCUTs for $\Delta=3.3$ and as a function of $J/J_\perp$. As expected, the various ranges CORE results agree with the ones obtained from PCUTs in the limit of small $J/J_\perp$, where both results are essentially exact. However, for $J/J_\perp\gtrsim0.15$ higher-order terms in the perturbative expansion start to dominate, invalidating the PCUTs analysis. Crucially, for the value $J/J_\perp=0.29$ considered in Refs. 18 and 19 (highlighted by the vertical dashed line in Fig. 6), the PCUTs expansion is clearly invalid, while longer-range CORE results are essentially converged.

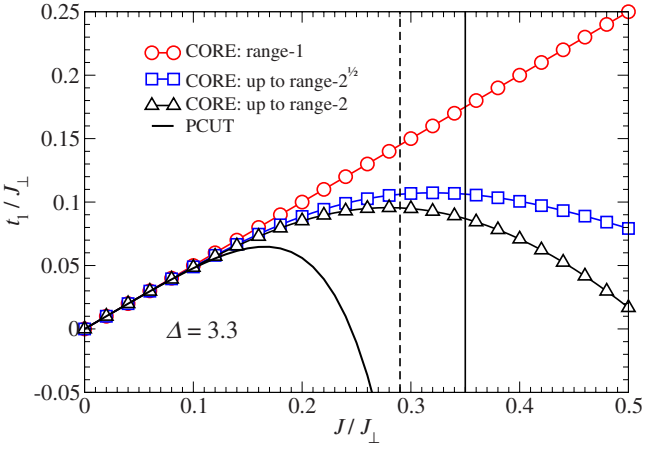

FIG. 6. (Color online) Comparison between CORE (range-1, -$2^{1/2}$ and -2) and PCUTs results for the nearest-neighbor hopping amplitude t_1 (for *particles*) in the effective bosonic model as a function of $J/J_\perp$ for $\Delta=3.3$, as in Refs. 18 and 19. The value $J/J_\perp=0.29$ is highlighted by the vertical dashed line. The vertical solid line indicates the point where longer-range ($2^{1/2}$ and 2) corrections to t_1 become larger than the range-1 contribution, signaling the breakdown of the CORE mapping (see main text).

TABLE I. Couplings in the effective Hamiltonian obtained from CORE [up to range-2, Eqs. (8) and (B1)–(B5)] for $\Delta=3.3$ and $J/J_\perp=0.29$. Also shown is the reduced NN hopping amplitude $\tilde{t}_1^{\mathrm{min}}$, defined by Eq. (10). Units are set by $J_\perp=1$.

$\tilde{\mu}^{\mathrm{C}}=2.911009-h$			
$\tilde{V}_1^{\mathrm{C}}$	0.336874	$\tilde{V}_2^{\mathrm{C}}$	−0.008851
$\tilde{V}_3^{\mathrm{C}}$	−0.011122	$\tilde{W}_1^{\mathrm{C}}$	0.009035
$\tilde{W}_2^{\mathrm{C}}$	−0.002257	$\tilde{W}_3^{\mathrm{C}}$	−0.064354
$\tilde{t}_1^{\mathrm{C}}$	0.145	$\tilde{t}_2^{\mathrm{C}}$	0
$\tilde{s}_1^{\mathrm{C}}$	−0.017190	$\tilde{s}_2^{\mathrm{C}}$	−0.021471
$\tilde{s}_3^{\mathrm{C}}$	−0.009378	$\tilde{s}_4^{\mathrm{C}}$	−0.000678
$\tilde{s}_5^{\mathrm{C}}$	−0.005367	$\tilde{s}_6^{\mathrm{C}}$	−0.009977
$\tilde{r}_1^{\mathrm{C}}$	0.000988	$\tilde{r}_2^{\mathrm{C}}$	−0.008850
$\tilde{t}_1^{\mathrm{min}}=0.130255$			

These results can be understood if we remark that any perturbative expansion about the weakly coupled dimer limit is only valid as long as one stays in the zero-field rung-singlet phase, with a finite gap to all three triplet modes. However, it has been shown[18,19] that for $\Delta=3.3$ and $J/J_\perp=0.29$ the zero-field ground state of the spin-dimer model [Eq. (1)] displays long-range Néel order implying the existence of a quantum critical point $J_c(h=0)/J_\perp<0.29$ (evident from poles in the Padé approximants for the perturbation series) beyond which our perturbative expansions become meaningless. On the other hand, although CORE relies on a strong dimerized character (so that dimer singlets and triplets are the relevant local degrees of freedom), it does not assume any particular ordering and therefore remains valid across the critical regime.

V. MECHANISM FOR SPIN SUPERSOLIDITY

Numerical values obtained from CORE for *all* effective couplings (up to range-2) appearing in Eqs. (8) and (B1)–(B5) are shown in Table I for the parameters $\Delta=3.3$, $J/J_\perp=0.29$ used in the original QMC simulations.[18,19] We use the MF approach discussed in Appendix C and calculate the dependence of the condensate density ρ_0 and CBS order parameter [see Eqs. (C4) and (C5)] on magnetic field h. The results are shown in Fig. 7(a). The semiquantitative agreement between estimates for the location of the quantum critical points obtained from the present analysis and from the QMC simulations for the original model [Eq. (1)] (shown in Fig. 2) is remarkable if we have in mind that only contributions of

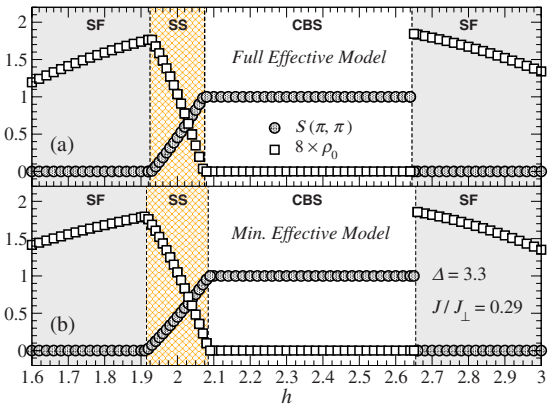

FIG. 7. (Color online) $\Delta=3.3$, $J/J_\perp=0.29$. Mean-field results for the CBS structure factor $S(\pi,\pi)$ (filled circles) and condensate density (Ref. 43) ρ_0 (open squares) as a function of the magnetic field h for: (a) the full range-2 CORE effective Hamiltonian, Eqs. (8) and (B1)–(B5), and (b) the minimal model of Eq. (9), with NN hopping amplitude given by Eq. (10). Values for the effective couplings are shown in Table I and successive phases are labeled as condensate, supersolid (SS), and checkerboard solid (CBS).

up to range-2 have been considered in the CORE calculation. However, MF approaches are known to overestimate supersolid behavior[9,10,17] and the effects of quantum fluctuations must be carefully analyzed.

Unfortunately, the effective Hamiltonian obtained from CORE, Eqs. (8) and (B1)–(B5), is complex and poses great challenges for more unbiased analysis. We therefore use the aforementioned MF procedure in gauging the relative importance of each term, with a twofold purpose: (a) identifying the dominant mechanism accounting for supersolidity in the spin-dimer model of Eq. (1) and (b) obtaining a simpler effective model amenable to QMC simulations (see below) in order to check whether the conjectured mechanisms survive after quantum fluctuations are taken into account.

A. Minimal Hamiltonian

In deciding on a minimal model we should obviously take into account the magnitudes associated with each term in Eqs. (8) and (B1)–(B5): we start by neglecting *all* effective couplings smaller than $0.1\tilde{t}_1^{\mathrm{C}}$, where $\tilde{t}_1^{\mathrm{C}}$ is the NN hopping for holes (singlets). Furthermore, since SS takes place only close to half-filling, we can also neglect the four-body term with coupling $\tilde{W}_3^{\mathrm{C}}$ [see Eq. (B2)]. The resulting model is identical to the second-order effective Hamiltonian [Eq. (5)],[25] but with strongly renormalized couplings. In particular, the couplings associated to the correlated hoppings $\tilde{s}_1^{\mathrm{C}}$ and $\tilde{s}_2^{\mathrm{C}}$ [see Figs. 3(a) and 3(b)] are considerably larger than predicted by the perturbative analysis,[25] as required for SS to emerge. However, the MF analysis of the resulting model shows that the extra kinetic energy associated to the large effective amplitudes for correlated hoppings requires the addition of the *attractive* two-body interactions $\tilde{V}_2^{\mathrm{C}}$ and $\tilde{V}_3^{\mathrm{C}}$ (see Table I) to stabilize a CBS plateau [cf. Figs. 10(a) and 10(b)]. These considerations lead to the *minimal model*:

$$\tilde{\mathcal{H}}_{\mathrm{min}}^{\mathrm{C}} = -\tilde{\mu}^{\mathrm{C}}\sum_i \tilde{n}_i + \sum_{\langle i,j\rangle}[\tilde{t}_1^{\mathrm{C}}(\tilde{b}_i^\dagger \tilde{b}_j + \mathrm{H.c.}) + \tilde{V}_1^{\mathrm{C}}\tilde{n}_i\tilde{n}_j] + \sum_{\langle\langle i,k\rangle\rangle}\{\tilde{s}_1^{\mathrm{C}}[\tilde{b}_i^\dagger(\tilde{n}_{j1}+\tilde{n}_{j2})\tilde{b}_k + \mathrm{H.c.}] + \tilde{V}_2^{\mathrm{C}}\tilde{n}_i\tilde{n}_k\} + \sum_{\langle\langle\langle i,l\rangle\rangle\rangle}[\tilde{s}_2^{\mathrm{C}}(\tilde{b}_i^\dagger \tilde{n}_j \tilde{b}_l + \mathrm{H.c.}) + \tilde{V}_3^{\mathrm{C}}\tilde{n}_i\tilde{n}_l]. \quad (9)$$

$\tilde{n}_i=\tilde{b}_i^\dagger\tilde{b}_i$ is the occupation number for *holes*; $\langle i,j\rangle$, $\langle\langle i,k\rangle\rangle$ and $\langle\langle\langle i,l\rangle\rangle\rangle$ denote, respectively, NN, NNN, and third-NN sites on the square lattice. The correlated hopping term with amplitude $\tilde{s}_1^{\mathrm{C}}$ [$\tilde{s}_2^{\mathrm{C}}$] is depicted in Fig. 3(a) [Fig. 3(b)]: a hole hops between two NNN [third-NN] sites i and k [l] only if at least one of their common NN sites $j1$, $j2$ [j] is occupied by a hole.[44]

Mean-field results (not shown) for the condensate density ρ_0 and the CBS order parameter $S(\pi,\pi)$ for the minimal model of Eq. (9), with effective couplings given in Table I (for $\Delta=3.3$ and $J/J_\perp=0.29$), semiquantitatively reproduce the QMC phase diagram (phase borders in Fig. 2) for the original spin-dimer model, Eq. (1). Unfortunately, this picture is too simplistic and results from QMC simulations (not shown) for this minimal model show that the CBS plateau is destroyed by quantum fluctuations, seemingly invalidating our analysis. However, the QMC results for $S(\pi,\pi)$ display a rather pronounced peak, indicating that our minimal model is close to a borderline where the solid phase appears: this is confirmed by the existence of an extended CBS plateau (concomitantly with a SS phase) in the QMC results obtained by considering *slightly* smaller values for the NN hopping amplitude $\tilde{t}_1^{\mathrm{C}}$,[45] suggesting that terms neglected in the full effective model [Eqs. (8) and (B1)–(B5)], although relatively small, play an important role.

A closer examination of the terms in the full effective CORE Hamiltonian [Eqs. (8) and (B1)–(B5)] neglected in deriving our minimal model [Eq. (9)] shows that the NN correlated hoppings with amplitudes $\tilde{s}_3^{\mathrm{C}}$ and $\tilde{s}_5^{\mathrm{C}}$ [see Eq. (B4) and Table I] have exactly the effect of decreasing the holes' (singlets') kinetic energy that may stabilize the CBS phase. However, the fact that $\tilde{t}_1^{\mathrm{C}}$ and $\tilde{s}_3^{\mathrm{C}}$, $\tilde{s}_5^{\mathrm{C}}$ have opposite signs also implies that their inclusion in Eq. (9) has the undesired effect that the resulting minimal model would suffer from the *sign problem*. In order to circumvent this problem and be able to perform QMC simulations, we incorporate $\tilde{s}_3^{\mathrm{C}}$ and $\tilde{s}_5^{\mathrm{C}}$ in an effective way: we notice that in a perfectly ordered CBS background these extra hoppings effectively reduce the NN hopping amplitude $\tilde{t}_1^{\mathrm{C}}$ to the value we denote $\tilde{t}_1^{\mathrm{min}}$ given by (to leading order)

$$\tilde{t}_1^{\mathrm{min}} = \tilde{t}_1^{\mathrm{C}} - (|\tilde{s}_3^{\mathrm{C}}| + |\tilde{s}_5^{\mathrm{C}}|). \quad (10)$$

MF results [Fig. 7(b)] for the new minimal effective model obtained by the substitution $\tilde{t}_1^{\mathrm{C}} \to \tilde{t}_1^{\mathrm{min}}$ in Eq. (9) suggests that the dominant physical processes are correctly taken into account, at least close to half-filling, as we can conclude from the excellent agreement with the results for the full effective CORE model [Fig. 7(a)].[46] Furthermore, the SS region visible in Fig. 7(b) is expected to survive quantum fluctuations, for a sizable leapfrog ratio $\Sigma(t_1^{\mathrm{min}}) \approx 0.43$ is obtained for Δ

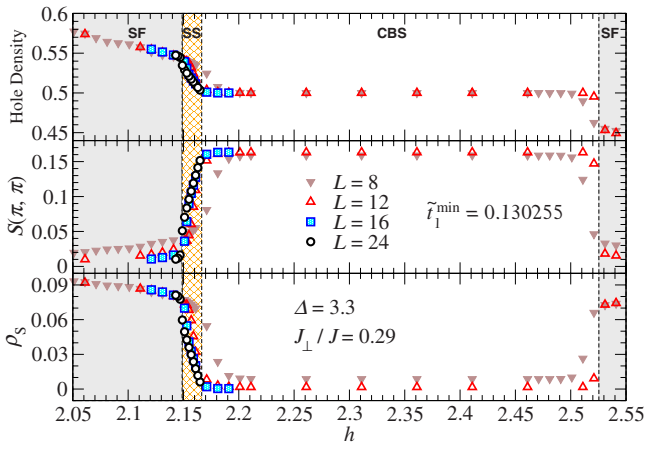

FIG. 8. (Color online) $\Delta=3.3$, $J/J_\perp=0.29$. QMC results for the minimal effective model obtained from CORE, Eq. (9), considering the NN hopping amplitude $\tilde{t}_1^{\min}$ from Eq. (10) (values for the couplings are given in Table I), for lattice sizes $L=8$, 12, 16 and 24. Error bars are much smaller than the depicted symbols. (a) Singlet density, (b) CBS order parameter $S(\pi,\pi)$ (Ref. 22) and (c) superfluid stiffness ρ_s (Ref. 43). The temperature is set to $T=1/20L<\tilde{t}_1^{\min}/2L$ (see main text). Successive phases are labeled as superfluid (SF), supersolid (SS), and checkerboard solid (CBS).

$=3.3$ and $J/J_\perp=0.29$, something confirmed by our QMC simulations below.

B. Quantum Monte Carlo simulations

We have performed QMC simulations, using an extended version[47] of the ALPS libraries' implementation[48,49] of the stochastic series expansion (SSE) algorithm.[50,51] We consider the minimal effective model of Eq. (9) with NN hopping amplitude $\tilde{t}_1^{\min}$ given by Eq. (10).[44] We evaluate the superfluid stiffness ρ_s,[43] obtained in terms of the winding numbers w_x and w_y,

$$\rho_s=\frac{1}{2\beta L^2}\langle w_x^2+w_y^2\rangle, \tag{11}$$

where β is the inverse temperature and L is the system size, and the CBS order parameter

$$S(\pi,\pi)=\frac{1}{L^2}\langle\sum_{\vec{r}_i,\vec{r}_j}(-1)^{\vec{r}_i-\vec{r}_j}\tilde{n}_{\vec{r}_i}\tilde{n}_{\vec{r}_j}\rangle, \tag{12}$$

as a function of the magnetic field h. Since we are interested in assessing ground-state properties, and the main kinetic energy scale in the minimal model Eq. (9) is $\tilde{t}_1^{\min}/J_\perp\approx 0.13$, we set the temperature to $T=1/20L<\tilde{t}_1^{\min}/2L$. It is important to remark that these temperatures are considerably lower than those considered by Ng and Lee,[18] who assumed that $J/J_\perp=0.29$ was the relevant energy scale, and this might explain the round shape observed in some of their curves.

QMC results for ρ_s and $S(\pi,\pi)$ for the minimal model of Eq. (9) with NN hopping amplitude given by Eq. (10), using the effective couplings appearing in Table I ($\Delta=3.3$ and $J/J_\perp=0.29$), are shown in Fig. 8. The overall agreement with QMC results for the original spin-dimer model [Eq. (1)],[18,19] shown in Fig. 2, is good and we can conclude that the minimal model of Eqs. (9) and (10) indeed accurately describes the low-energy physics of the original model and, more importantly, that the "leapfrog mechanism" presented in Sec. II is at least partially responsible for spin-supersolid behavior.

Although the just presented results show that the essential ingredients for spin supersolidity have been identified, it is clear that quantitative agreement is not achieved. Specifically, the extent of the SS phase is considerably smaller in Fig. 8 than in Fig. 2; reversely, the CBS phase in the former is about twice as large than in the latter. In trying to understand this mismatch it is important to keep in mind that supersolidity emerges in this model as the result of a delicate balance between kinetic and interaction terms. This is evident in the MF analysis discussed in Sec. V A, which suggests that the effective model obtained from CORE is close to a borderline and that small variations in the effective couplings can have drastic effects. For instance, we have shown that the minimal model [Eq. (9)], with effective couplings shown in Table I, does not display a CBS phase; however, by replacing $\tilde{t}_1^{\mathrm{C}}\to\tilde{t}_1^{\min}$ [Eq. (10)] we obtain a CBS phase twice as large as expected.

Therefore, and since the *sign problem* precludes us from performing QMC simulations for the full effective Hamiltonian [Eqs. (8) and (B1)–(B5)], we conjecture that terms ignored in obtaining the minimal model [Eqs. (9) and (10)], even with small couplings, must be included in order to better reproduce the results for the original model, shown in Fig. 2. Additionally, the NN correlated hoppings with amplitudes $\tilde{s}_3^{\mathrm{C}}$ and $\tilde{s}_5^{\mathrm{C}}$ appear to favor SS and the fact that we include only their effects in reducing $\tilde{t}_1^{\mathrm{C}}$ [Eq. (10)] might be responsible for the reduced SS phase in Fig. 8.[46] Finally, it is not possible to exclude the possibility that longer-range effective interactions and/or neglected triplet excitations ($|t^0\rangle$, $|t^{-1}\rangle$) may be required for obtaining quantitative agreement.

C. Extent of the supersolid phase

We have extended our MF analysis to the full effective model [Eqs. (8) and (B1)–(B5)] by varying the parameters Δ and $J/J_\perp$, as a function of the magnetic field h. Results are shown in Fig. 9. Gray shaded areas represent values of Δ and $J/J_\perp$ for which no SS phase is stabilized within MF for all values of h and only a superfluid and/or CBS phases are obtained. However, SS does appear over an extended region in the parameter space within MF. Since it is well known that MF tends to overestimate supersolidity, we have also analyzed the "leapfrog ratio" $\Sigma(t_1^{\min})$ [see Eq. (2)] throughout the parameter space. As discussed in Sec. II, the condition $\Sigma(t_1^{\min})>c/4$, with $c\in[1,2]$, must be satisfied for preventing phase separation and stabilizing a SS. Regions for which this condition is fulfilled are indicated in Fig. 9: we can see that the region where the SS phase is likely to occur is much smaller than expected from the MF analysis and, in particular, no SS is expected within the perturbative limit.

VI. CONCLUSIONS AND OUTLOOK

Summarizing, we have obtained effective models describing the low-energy physics of a spin-dimer model [Eq. (1)]

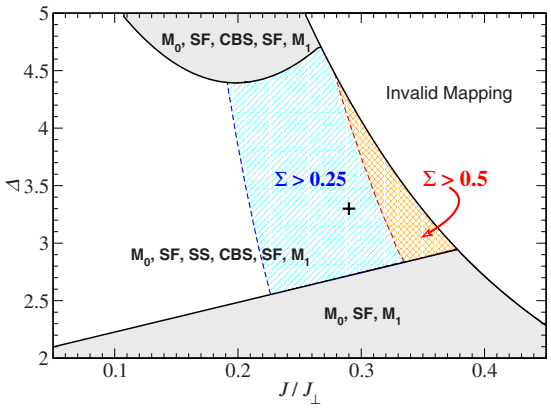

FIG. 9. (Color online) Successive phases stabilized for increasing magnetic field h in the parameter space of the spin-dimer model of Eq. (1), as obtained from a mean-field analysis of the full CORE Hamiltonian, Eqs. (8) and (B1)–(B5). Gray shaded areas correspond to parameters for which no supersolid phase is found and in the region marked as "invalid mapping" the CORE expansion is invalid (see Sec. IV A). In the remaining area a supersolid phase is obtained within the mean-field approach. The colorful regions indicate parameters for which the singlet "leapfrog ratio" [Eq. (2)] is larger than the threshold value $\Sigma(\tilde{t}_1^{\min}) > c/4$ (with $c \in [1,2]$), as required for SS phases to appear. The cross highlights parameters $\Delta=3.3$ and $J/J_\perp=0.29$ from Refs. 18 and 19. Phases are labeled as Mott insulator (M_0, empty, and M_1, full), superfluid (SF), supersolid (SS), and checkerboard solid (CBS).

known to exhibit spin-supersolid behavior[18,19] with the help of perturbative expansions and of the CORE algorithm. While the perturbative analysis, relying on the assumption of a disordered ground state with gapped excitations at zero field, does not reproduce the extended supersolid phase observed in the original model (Fig. 2), CORE does not assume any particular ordering in the system and is shown to reproduce the main features obtained from more computationally demanding approaches, even when a simple mean-field procedure is applied to the obtained effective model.

Furthermore, we identify the mechanism at play behind spin supersolidity and we show that the spin-supersolid phase exhibited by the $S=1/2$ spin-dimer model of Eq. (1) can be simply understood in terms of the "leapfrog mechanism" illustrated in Fig. 3. Basically, a sizable amplitude for correlated hoppings allow extra holes (singlets) to delocalize on the other sublattice of a checkerboard solid, preventing phase separation and leading to supersolid behavior.

More generally speaking, we are able to describe the physics behind complex phenomena in a simple way by deriving effective models with only a few terms and rather local couplings. The essential physical ingredients can be identified even in a low-order perturbative analysis, although more sophisticated approaches, such as PCUTs and CORE, may be required in obtaining the effective couplings. We highlight that both PCUTs and CORE are immune to the *sign problem* and can therefore be applied to frustrated and fermionic systems, something which opens interesting research possibilities.

ACKNOWLEDGMENTS

We acknowledge the financial support of the Swiss National Fund and of MaNEP. A.F.A. is indebted to A. Abendschein for sharing numerical results and for fruitful discussions and acknowledges financial support from CNPq (Brazil), NIDECO (Switzerland), and ARC (Australia). K.P.S. acknowledges ESF and EuroHorcs for funding through his EURYI. N.L. acknowledges the Laboratoire de Physique Théorique (Toulouse) for hospitality. F.M. acknowledges the Région Midi-Pyrénées through its Chaire d'excellence Pierre de Fermat program for financial support and thanks the Laboratoire de Physique Théorique (Toulouse) for hospitality.

APPENDIX A: PCUTS SIXTH-ORDER EFFECTIVE COUPLINGS

The effective couplings obtained from the PCUTs analysis discussed in Sec. III B are

$$t_1^{\mathrm{P6}} = \frac{1}{2}J - \frac{5}{32}J^3 - \frac{3}{32}J^3\Delta^2 - \frac{13}{32}J^4\Delta - \frac{1}{16}J^4\Delta^3 - \frac{265}{512}J^5 - \frac{61}{512}J^5\Delta^2 - \frac{57}{256}J^5\Delta^4 - \frac{393}{1024}J^6\Delta + \frac{193}{1024}J^6\Delta^3 - \frac{15}{64}J^6\Delta^5,$$

$$V_1^{\mathrm{P6}} = \frac{1}{2}J\Delta - \frac{1}{4}J^2 - \frac{1}{8}J^2\Delta^2 - \frac{3}{16}J^3\Delta - \frac{95}{128}J^4 + \frac{79}{128}J^4\Delta^2 - \frac{51}{128}J^4\Delta^4 - \frac{395}{1024}J^5\Delta + \frac{191}{1024}J^5\Delta^3 - \frac{14937}{8192}J^6 + \frac{11545}{16384}J^6\Delta^2 + \frac{32641}{16384}J^6\Delta^4 - \frac{419}{256}J^6\Delta^6,$$

$$t_2^{\mathrm{P6}} = -\frac{1}{4}J^2 - \frac{1}{4}J^3\Delta + \frac{1}{16}J^4 + \frac{1}{32}J^4\Delta^2 + \frac{1}{2}J^5\Delta + \frac{3}{32}J^5\Delta^3 + \frac{63}{128}J^6 + \frac{45}{256}J^6\Delta^2 + \frac{171}{512}J^6\Delta^4,$$

$$t_2'^{\mathrm{P6}} = \frac{1}{8}J^2 + \frac{5}{32}J^3\Delta - \frac{35}{256}J^4 - \frac{3}{128}J^4\Delta^2 - \frac{1089}{2048}J^5\Delta - \frac{77}{1024}J^5\Delta^3 - \frac{3025}{4096}J^6 - \frac{3623}{16384}J^6\Delta^2 - \frac{5737}{16384}J^6\Delta^4. \tag{A1}$$

APPENDIX B: EFFECTIVE COUPLINGS FROM CORE

The explicit expressions for each term in the effective Hamiltonian obtained from CORE, Eq. (8), are given here (in the expressions below $\tilde{n}_i=\tilde{b}_i^\dagger\tilde{b}_i$ is the occupation number for *holes* and $\hat{x},\hat{y}$ are unity vectors for the square lattice; constant terms arising from applying a particle-hole transfor-

mation to the bare CORE effective Hamiltonian are ignored). $\tilde{\mathcal{V}}$ comprises two-body interactions

$$\tilde{\mathcal{V}}_i = \tilde{V}_1^{\mathrm{C}}(\tilde{n}_i\tilde{n}_{i+\hat{x}} + \tilde{n}_i\tilde{n}_{i+\hat{y}}) + \tilde{V}_2^{\mathrm{C}}(\tilde{n}_i\tilde{n}_{i+\hat{x}+\hat{y}} + \tilde{n}_i\tilde{n}_{i+\hat{x}-\hat{y}}) + \tilde{V}_3^{\mathrm{C}}(\tilde{n}_i\tilde{n}_{i+2\hat{x}} + \tilde{n}_i\tilde{n}_{i+2\hat{y}}), \tag{B1}$$

and $\tilde{\mathcal{W}}$ three- and four-body interactions

$$\tilde{\mathcal{W}}_i = \tilde{W}_1^{\mathrm{C}}(\tilde{n}_i\tilde{n}_{i+\hat{x}}\tilde{n}_{i+2\hat{x}} + \tilde{n}_i\tilde{n}_{i+\hat{y}}\tilde{n}_{i+2\hat{y}}) + \tilde{W}_2^{\mathrm{C}}[\tilde{n}_i\tilde{n}_{i+\hat{x}}(\tilde{n}_{i+\hat{y}} + \tilde{n}_{i+\hat{x}+\hat{y}} + \tilde{n}_{i-\hat{y}} + \tilde{n}_{i+\hat{x}-\hat{y}})] + \tilde{W}_3^{\mathrm{C}}(\tilde{n}_i\tilde{n}_{i+\hat{x}}\tilde{n}_{i+\hat{y}}\tilde{n}_{i+\hat{x}+\hat{y}}). \tag{B2}$$

The effective single-boson hopping terms in Eq. (8) are

$$\tilde{\mathcal{T}}_i = \tilde{t}_1^{\mathrm{C}}(\tilde{b}_i^\dagger\tilde{b}_{i+\hat{x}} + \tilde{b}_i^\dagger\tilde{b}_{i+\hat{y}} + \mathrm{H.c.}) + \tilde{t}_2^{\mathrm{C}}(\tilde{b}_i^\dagger\tilde{b}_{i+\hat{x}+\hat{y}} + \tilde{b}_i^\dagger\tilde{b}_{i+\hat{x}-\hat{y}} + \mathrm{H.c.}). \tag{B3}$$

Correlated hopping terms are

$$\begin{aligned}\tilde{\mathcal{S}}_i = {} & \tilde{s}_1^{\mathrm{C}}[\tilde{b}_i^\dagger(\tilde{n}_{i+\hat{x}} + \tilde{n}_{i+\hat{y}})\tilde{b}_{i+\hat{x}+\hat{y}} + \tilde{b}_i^\dagger(\tilde{n}_{i+\hat{x}} + \tilde{n}_{i-\hat{y}})\tilde{b}_{i+\hat{x}-\hat{y}} + \mathrm{H.c.}] \\ & + \tilde{s}_2^{\mathrm{C}}[\tilde{b}_i^\dagger\tilde{n}_{i+\hat{x}}\tilde{b}_{i+2\hat{x}} + \tilde{b}_i^\dagger\tilde{n}_{i+\hat{y}}\tilde{b}_{i+2\hat{y}} + \mathrm{H.c.}] + \tilde{s}_3^{\mathrm{C}}[\tilde{b}_i^\dagger\tilde{b}_{i+\hat{x}}(\tilde{n}_{i+\hat{y}} \\ & + \tilde{n}_{i+\hat{x}+\hat{y}} + \tilde{n}_{i-\hat{y}} + \tilde{n}_{i+\hat{x}-\hat{y}}) + \tilde{b}_i^\dagger\tilde{b}_{i+\hat{y}}(\tilde{n}_{i+\hat{x}} + \tilde{n}_{i+\hat{x}+\hat{y}} + \tilde{n}_{i-\hat{x}} \\ & + \tilde{n}_{i-\hat{x}+\hat{y}}) + \mathrm{H.c.}] + \tilde{s}_4^{\mathrm{C}}[\tilde{b}_i^\dagger\tilde{b}_{i+\hat{x}}(\tilde{n}_{i+\hat{y}}\tilde{n}_{i+\hat{x}+\hat{y}} + \tilde{n}_{i-\hat{y}}\tilde{n}_{i+\hat{x}-\hat{y}}) \\ & + \tilde{b}_i^\dagger\tilde{b}_{i+\hat{y}}(\tilde{n}_{i+\hat{x}}\tilde{n}_{i+\hat{x}+\hat{y}} + \tilde{n}_{i-\hat{x}}\tilde{n}_{i-\hat{x}+\hat{y}}) + \mathrm{H.c.}] \\ & + \tilde{s}_5^{\mathrm{C}}[\tilde{b}_i^\dagger\tilde{b}_{i+\hat{x}}(\tilde{n}_{i-\hat{x}} + \tilde{n}_{i+2\hat{x}}) + \tilde{b}_i^\dagger\tilde{b}_{i+\hat{y}}(\tilde{n}_{i-\hat{y}} + \tilde{n}_{i+2\hat{y}}) + \mathrm{H.c.}] \\ & + \tilde{s}_6^{\mathrm{C}}(\tilde{b}_i^\dagger\tilde{n}_{i+\hat{x}}\tilde{n}_{i+\hat{y}}\tilde{b}_{i+\hat{x}+\hat{y}} + \tilde{b}_i^\dagger\tilde{n}_{i+\hat{x}}\tilde{n}_{i-\hat{y}}\tilde{b}_{i+\hat{x}-\hat{y}} + \mathrm{H.c.}),\end{aligned} \tag{B4}$$

and, finally, hoppings simultaneously involving two-bosons

$$\tilde{\mathcal{R}}_i = \tilde{r}_1^{\mathrm{C}}(\tilde{b}_i^\dagger\tilde{b}_{i+\hat{x}}^\dagger\tilde{b}_{i+\hat{y}}\tilde{b}_{i+\hat{x}+\hat{y}} + \tilde{b}_i^\dagger\tilde{b}_{i+\hat{y}}^\dagger\tilde{b}_{i+\hat{x}}\tilde{b}_{i+\hat{x}+\hat{y}} + \mathrm{H.c.}) + \tilde{r}_2^{\mathrm{C}}(\tilde{b}_i^\dagger\tilde{b}_{i+\hat{x}}\tilde{b}_{i+\hat{y}}\tilde{b}_{i+\hat{x}+\hat{y}}^\dagger + \tilde{b}_i^\dagger\tilde{b}_{i+\hat{x}}\tilde{b}_{i-\hat{y}}\tilde{b}_{i+\hat{x}-\hat{y}}^\dagger + \mathrm{H.c.}). \tag{B5}$$

APPENDIX C: MEAN-FIELD PROCEDURE

Following the Matsubara-Matsuda semiclassical approach,[52] we write the hard-core boson effective models in terms of $S=1/2$ pseudospin variables. We start by replacing the commutation relations for bosons on the same site i,

$$[b_i, b_i] = [b_i^\dagger, b_i^\dagger] = 0 \quad \text{and} \quad [b_i, b_i^\dagger] = 1, \tag{C1}$$

by the fermionic anticommutation relations

$$\{b_i, b_i\} = \{b_i^\dagger, b_i^\dagger\} = 0 \quad \text{and} \quad \{b_i, b_i^\dagger\} = 1, \tag{C2}$$

while retaining the canonical bosonic commutators for operators on different sites i,j. This leads to an algebra formally equivalent to that of a spin 1/2.

We then neglect quantum fluctuations by replacing the pseudospin operators by their mean value, obtaining a Hamiltonian in terms of classical spin variables $\mathbf{S} = (\cos\phi \sin\theta, \sin\phi \sin\theta, \cos\theta)$ which reads

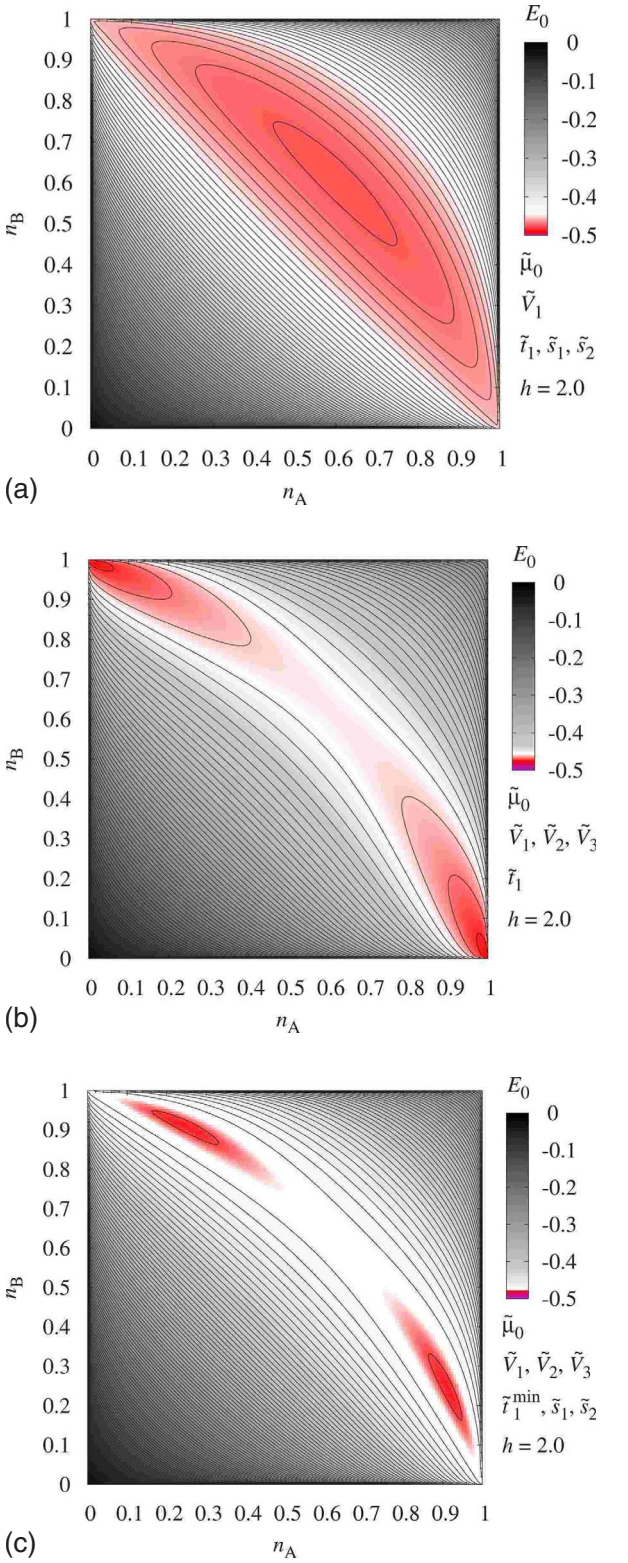

FIG. 10. (Color online) $\Delta=3.3$, $J/J_\perp=0.29$ and $h=2$. Mean-field ground-state energy per site, E_0, for "partial" effective models comprising the following terms [see Eq. (9); values for the effective couplings are shown in Table I]: (a) $\tilde{\mu}^{\mathrm{C}}$, $\tilde{V}_1^{\mathrm{C}}$, $\tilde{t}_1^{\mathrm{C}}$, $\tilde{s}_1^{\mathrm{C}}$ and $\tilde{s}_2^{\mathrm{C}}$, leading to a superfluid phase. (b) $\tilde{\mu}^{\mathrm{C}}$, $\tilde{V}_1^{\mathrm{C}}$, $\tilde{V}_2^{\mathrm{C}}$, $\tilde{V}_3^{\mathrm{C}}$ and $\tilde{t}_1^{\mathrm{C}}$, leading to a CBS phase. (c) The minimal model from Eqs. (9) and (10), for which a spin-supersolid phase is obtained [cf. Fig. 7(b)].

$$\mathcal{H}_{\mathrm{MF}} = h_{\mathrm{eff}} \sum_i S_i^z + \sum_{\langle i,j\rangle} [\tilde{J}_{ij}^z S_i^z S_j^z + \tilde{J}_{ij}^{\perp}(S_i^x S_j^x + S_i^y S_j^y)]$$
$$+ \sum_{\langle i,j,k\rangle} [\tilde{K}_{ijk}^{\perp} S_i^z (S_j^x S_k^x + S_j^y S_k^y) + \tilde{K}_{ijk}^z S_i^z S_j^z S_k^z]$$
$$+ \sum_{\langle i,j,k,l\rangle} [\tilde{L}_{ijkl}^{\perp} S_i^z S_j^z (S_k^x S_l^x + S_k^y S_l^y) + \tilde{L}_{ijkl}^z S_i^z S_j^z S_k^z S_l^z]$$
$$+ \sum_{\langle i,j,k,l\rangle} [\tilde{M}_{ijkl}^{\perp}(S_i^+ S_j^- S_k^+ S_l^- + \mathrm{H.c.})]. \quad \text{(C3)}$$

The parameters h_{eff} (one-body), $\tilde{J}$ (two-body), $\tilde{K}$ (three-body), $\tilde{L}$ (four-body) and $\tilde{M}$ (double exchange) are defined in terms of the couplings in the effective bosonic Hamiltonian. The superscript z ($\perp$) accounts for interactions (hoppings) between sites coupled as in the bosonic Hamiltonian.

In accounting for the different phases of the Hamiltonian Eq. (1) it suffices to consider a site-factorized wave-function $|\psi\rangle = \Pi_i |\psi_i\rangle$ assuming two-sublattice long-range order ($i = A, B$). The variational parameters (ϕ_A, ϕ_B, θ_A, and θ_B) are determined by minimizing the ground-state energy per site within this subspace. The condensate density[43] corresponds in a MF approach to the magnetization in the xy plane

$$\rho_0 = \frac{1}{8}(\sin^2\theta_A + \sin^2\theta_B), \quad \text{(C4)}$$

and the CBS structure factor is

$$S(\pi,\pi) = (\cos\theta_A - \cos\theta_B)^2/4. \quad \text{(C5)}$$

In terms of the density of singlets in the sublattice A, given by

$$n_A = \frac{1+\cos\theta_A}{2}, \quad \text{(C6)}$$

with a similar definition for the sublattice B (n_B), the ground-state energy per site E_0 (up to a constant) for the minimal model of Eqs. (9) and (10) is

$$E_0 = 2\tilde{V}_1^{\mathrm{C}} n_A n_B \quad \text{(C7)}$$
$$+ (\tilde{V}_2^{\mathrm{C}} + \tilde{V}_3^{\mathrm{C}})(n_A^2 + n_B^2) \quad \text{(C8)}$$
$$+ 4\tilde{t}_1^{\mathrm{C}} \sqrt{n_A(1-n_A)}\sqrt{n_B(1-n_B)}\cos(\phi_A - \phi_B) \quad \text{(C9)}$$
$$+ 2(\tilde{s}_2^{\mathrm{C}} + 2\tilde{s}_1^{\mathrm{C}}) n_A n_B (2 - n_B - n_A) \quad \text{(C10)}$$
$$+ (h-\mu)\frac{n_A + n_B}{2}. \quad \text{(C11)}$$

We can therefore deduce the following trends:

(i) The kinetic term associated to the NN hopping amplitude $\tilde{t}_1^{\mathrm{C}}$, Eq. (C9), favors a SF phase, since it is minimized for $n_A = n_B$ and $\phi_A - \phi_B = \pi$. Thus, there is no symmetry breaking between A and B sublattices and the latter relation introduces order in the xy plane, a *condensate* within the present semiclassical treatment. This trend is illustrated in Fig. 10(a), where the ground-state energy per site E_0 is plotted as a function of the densities n_A and n_B for a "partial" effective model comprising the following terms (see Sec. V A): $\tilde{\mu}^{\mathrm{C}}$, $\tilde{V}_1^{\mathrm{C}}$, $\tilde{t}_1^{\mathrm{C}}$, $\tilde{s}_1^{\mathrm{C}}$, and $\tilde{s}_2^{\mathrm{C}}$.

(ii) Effective singlet interactions, $\tilde{V}_1^{\mathrm{C}}$, $\tilde{V}_2^{\mathrm{C}}$, and $\tilde{V}_3^{\mathrm{C}}$, favor a CBS phase and their contribution to the ground-state energy [Eqs. (C7) and (C8)] is minimized if the $A-B$ symmetry is broken. This is shown in Fig. 10(b), where the following effective couplings were considered: $\tilde{\mu}^{\mathrm{C}}$, $\tilde{V}_1^{\mathrm{C}}$, $\tilde{V}_2^{\mathrm{C}}$, $\tilde{V}_3^{\mathrm{C}}$, and $\tilde{t}_1^{\mathrm{C}}$.

(iii) A compromise between the two previous trends (supersolidity) is achieved by including the correlated hopping terms with amplitudes $\tilde{s}_1^{\mathrm{C}}$ and $\tilde{s}_2^{\mathrm{C}}$ [Eq. (C10)]. While if considered separately this purely kinetic contribution does not break the translational symmetry and only favors the SF phase, adding it to a configuration already leading to a CBS may stabilize a supersolid, as shown in Fig. 10(c) for the minimal model from Eqs. (9) and (10): the $A-B$ symmetry is broken concomitantly with ordering in the xy plane ($\phi_A - \phi_B = \pi$).

For the sake of completeness, we now analyze the NN correlated hoppings with amplitudes $\tilde{s}_3^{\mathrm{C}}$ and $\tilde{s}_5^{\mathrm{C}}$, employed in defining $\tilde{t}_1^{\mathrm{min}}$ [Eq. (10)] and that cannot be investigated by means of QMC simulations. Their contribution to the MF ground-state energy reads

$$+ 4(\tilde{s}_3^{\mathrm{C}} + 2\tilde{s}_5^{\mathrm{C}})\sqrt{n_A n_B (1-n_B)(1-n_A)} \cdot (n_A + n_B)\cos(\phi_A - \phi_B). \quad \text{(C12)}$$

If considered alone, this term is minimized for $\phi_A = \phi_B$ and there is no breaking of the $A-B$ symmetry. However, if $\phi_A - \phi_B = \pi$, as imposed by the much larger contribution due to the uncorrelated NN hopping $\tilde{t}_1^{\mathrm{C}}$ [Eq. (C9)], Eq. (C12) favors supersolidity and $A-B$ symmetry is broken even if interactions are not taken into account (within our MF approach). This is to be contrasted with the case of the longer-range correlated hoppings $\tilde{s}_1^{\mathrm{C}}$ and $\tilde{s}_2^{\mathrm{C}}$ [Eq. (C10)].

[1] T. Giamarchi, C. Rüegg, and O. Tchernyshyov, Nat. Phys. **4**, 198 (2008).
[2] E. Kim and M. H. W. Chan, Nature (London) **427**, 225 (2004).
[3] E. Kim and M. H. W. Chan, Science **305**, 1941 (2004).
[4] S. Sasaki, R. Ishiguro, F. Caupin, H. J. Maris, and S. Balibar, Science **313**, 1098 (2006).
[5] J.-P. Bouchaud and G. Biroli, arXiv:0710.3087 (unpublished).
[6] L. Pollet, M. Boninsegni, A. B. Kuklov, N. V. Prokof'ev, B. V. Svistunov, and M. Troyer, Phys. Rev. Lett. **98**, 135301 (2007).
[7] L. Pollet, M. Boninsegni, A. B. Kuklov, N. V. Prokof'ev, B. V. Svistunov, and M. Troyer, Phys. Rev. Lett. **101**, 097202 (2008).
[8] G. G. Batrouni and R. T. Scalettar, Phys. Rev. Lett. **84**, 1599 (2000).
[9] G. Schmid, S. Todo, M. Troyer, and A. Dorneich, Phys. Rev.

Lett. **88**, 167208 (2002).
[10] P. Sengupta, L. P. Pryadko, F. Alet, M. Troyer, and G. Schmid, Phys. Rev. Lett. **94**, 207202 (2005).
[11] S. Wessel and M. Troyer, Phys. Rev. Lett. **95**, 127205 (2005).
[12] D. Heidarian and K. Damle, Phys. Rev. Lett. **95**, 127206 (2005).
[13] R. G. Melko, A. Paramekanti, A. A. Burkov, A. Vishwanath, D. N. Sheng, and L. Balents, Phys. Rev. Lett. **95**, 127207 (2005).
[14] M. Boninsegni and N. V. Prokof'ev, Phys. Rev. Lett. **95**, 237204 (2005).
[15] G. G. Batrouni, F. Hébert, and R. T. Scalettar, Phys. Rev. Lett. **97**, 087209 (2006).
[16] Y. C. Chen, R. G. Melko, S. Wessel, and Y. J. Kao, Phys. Rev. B **77**, 014524 (2008).
[17] K. P. Schmidt, J. Dorier, A. M. Läuchli, and F. Mila, Phys. Rev. Lett. **100**, 090401 (2008).
[18] K.-K. Ng and T. K. Lee, Phys. Rev. Lett. **97**, 127204 (2006).
[19] N. Laflorencie and F. Mila, Phys. Rev. Lett. **99**, 027202 (2007).
[20] P. Sengupta and C. D. Batista, Phys. Rev. Lett. **98**, 227201 (2007).
[21] P. Sengupta and C. D. Batista, Phys. Rev. Lett. **99**, 217205 (2007).
[22] Plotted QMC results for the CBS structure factor $S(\pi,\pi)$ both for the spin-dimer model of Eq. (1) (Fig. 2) and for the minimal effective model [Eqs. (9) and (10)] (shown in Fig. 8) have been renormalized so that a perfectly ordered CBS plateau would lead to $S(\pi,\pi)=1$, as within our MF approach, Eq. (C5). In this way, we can see that $S(\pi,\pi)$ is reduced to $\sim 60-70\%$ of its classical value when quantum fluctuations are taken into account.
[23] K. Totsuka, Phys. Rev. B **57**, 3454 (1998).
[24] F. Mila, Eur. Phys. J. B **6**, 201 (1998).
[25] To second order in $J/J_\perp$, the processes appearing in Figs. 3(a) and 3(b) have the same amplitude. This is not the case for the effective Hamiltonian obtained from CORE; see Table I.
[26] F. Wegner, Ann. Phys. **77**, 3 (1994).
[27] S. D. Głazek and K. G. Wilson, Phys. Rev. D **48**, 5863 (1993).
[28] S. D. Glazek and K. G. Wilson, Phys. Rev. D **49**, 4214 (1994).
[29] C. Knetter, K. P. Schmidt, M. Grüninger, and G. S. Uhrig, Phys. Rev. Lett. **87**, 167204 (2001).
[30] J. Stein, J. Stat. Phys. **88**, 487 (1997).
[31] A. Mielke, Eur. Phys. J. B **5**, 605 (1998).
[32] G. S. Uhrig and B. Normand, Phys. Rev. B **58**, R14705 (1998).
[33] C. Knetter and G. S. Uhrig, Eur. Phys. J. B **13**, 209 (2000).
[34] F. Mila and K. P. Schmidt, Springer Ser. Solid-State Sci. (to be published).
[35] J. Dorier, K. P. Schmidt, and F. Mila, arXiv:0806.3406, Phys. Rev. Lett. (to be published).
[36] C. Knetter, K. P. Schmidt, and G. S. Uhrig, J. Phys. A **36**, 7889 (2003).
[37] C. J. Morningstar and M. Weinstein, Phys. Rev. Lett. **73**, 1873 (1994).
[38] C. J. Morningstar and M. Weinstein, Phys. Rev. D **54**, 4131 (1996).
[39] A. Abendschein and S. Capponi, Phys. Rev. B **76**, 064413 (2007).
[40] E. Altman and A. Auerbach, Phys. Rev. B **65**, 104508 (2002).
[41] S. Capponi, Theor. Chem. Acc. **116**, 524 (2006).
[42] S. Capponi, A. Läuchli, and M. Mambrini, Phys. Rev. B **70**, 104424 (2004).
[43] We remark that it is nontrivial to quantitatively relate the condensate density ρ_0 [density of particles occupying the lowest energy mode, obtained within our MF procedure from Eq. (C4)] and the superfluid stiffness ρ_s [that measures the system's phase coherence and is obtained in terms of winding numbers in the QMC simulations, Eq. (11)]. For a discussion of how ρ_0, ρ_s and the superfluid density are related, the reader is referred to Refs. 53 and 54; in the present case, this issue is further complicated by the presence of correlated hopping terms in the effective Hamiltonian Eq. (9). However, we stress that the comparison between different results for the location of the SS phase suffices for concluding on the mechanism for spin supersolidity in the model [Eq. (1)], the goal of the present study.
[44] It is interesting to note that the effective uncorrelated hoppings for holes with range-$2^{1/2}$ (NNN) and -2 (third-neighbor) have zero amplitude within the CORE approach and therefore cannot account for supersolidity in the spin-dimer model, Eq. (1). Accordingly, they are not present in the minimal model, Eq. (9), which therefore does not suffer from the sign problem.
[45] By reducing $\tilde{t}_1^{\mathrm{C}}$ from the starting value 0.145 and keeping all the other couplings appearing in Eq. (9) unchanged, CBS and SS already appear for $\tilde{t}_1^{\mathrm{C}} \sim 0.14$.
[46] A MF analysis for the enlarged minimal model including, besides terms appearing in Eq. (9), the correlated hopping terms with amplitudes $\tilde{s}_3^{\mathrm{C}}$ and $\tilde{s}_5^{\mathrm{C}}$ [Eq. (B4)], reveals an enlarged SS region (compared with the one obtained for the full effective model). This suggests that the terms with amplitudes $\tilde{s}_3^{\mathrm{C}}$ and $\tilde{s}_5^{\mathrm{C}}$ play a role in stabilizing SS and the fact that they are not explicitly included in the minimal model [Eq. (9)] might explain the shrunk SS region in our QMC results.
[47] K. P. Schmidt, J. Dorier, A. Läuchli, and F. Mila, Phys. Rev. B **74**, 174508 (2006).
[48] F. Alet, S. Wessel, and M. Troyer, Phys. Rev. E **71**, 036706 (2005).
[49] F. Alet *et al.*, J. Phys. Soc. Jpn. Suppl. **74**, 30 (2005).
[50] A. W. Sandvik, Phys. Rev. B **59**, R14157 (1999).
[51] O. F. Syljuåsen and A. W. Sandvik, Phys. Rev. E **66**, 046701 (2002).
[52] T. Matsubara and H. Matsuda, Prog. Theor. Phys. **16**, 569 (1956).
[53] M. E. Fisher, M. N. Barber, and D. Jasnow, Phys. Rev. A **8**, 1111 (1973).
[54] K. Bernardet, G. G. Batrouni, J.-L. Meunier, G. Schmid, M. Troyer, and A. Dorneich, Phys. Rev. B **65**, 104519 (2002).